LASER & PHOTONICS REVIEWS
www.lpr-journal.org

Liquid-Crystal-Enabled Varifocal Achromatic Metalens

Qiguang Wang, Yaqian Xu, Zhenghao Guo, Li Chen, Chunyu Huang, and Wei Hu**

Integrated planar optical devices with dynamic functionalities are in high demand in the rapidly developing terahertz region. In particular, varifocal achromatic metalenses are urgently needed for biochemical discrimination imaging and nondestructive inspection. Here, a design is proposed to realize a varifocal achromatic metalens. It works on the simultaneous compensation of the diffraction dispersion of a foci-switchable basic phase profile on the basis of a properly preset group delay of a propagation phase. The concept is demonstrated with a liquid crystal integrated silicon metalens. The major axis orientation of cylindroid meta-atoms supplies a fixed geometric phase, the photopatterned liquid crystal provides a switchable geometric phase, and the compensation originates from the shape variation of cylindroid meta-atoms. Both simulations and experiments verify the switchable achromatic focusing at two distinct foci (10.20 and 13.76 mm) across 1.0–1.6 THz. Dual-depth multispectral imaging is further demonstrated with two medicaments, exhibiting its potential for nondestructive safety screening and pharmaceutical identification. The proposed strategy establishes a framework for next-generation adaptive terahertz techniques and applications.

1. Introduction

The removal of chromatic aberration is of primary importance in optical imaging systems. Metadevices such as metalenses spatially modulate electromagnetic waves within an ultrathin layer, embracing the trend of miniaturization and integration of modern optics.[1,2] However, traditional metalenses suffer from intensive diffractive dispersion, severely hindering their corresponding investigations and applications. To overcome this challenge, significant progress has been made during the past few years. Dispersion was successfully compensated via the introduction of distinct phase species,[3] the cascading of specially designed layers for narrowband light modulations,[4] and inverse design.[5] Most of the above strategies have been demonstrated only in optical[6–9] or near-IR[10,11] bands. The chromatic aberration of terahertz (THz) metalens is more challenging due to the broadband nature of the THz spectrum.[12] THz wave is pivotal in future wireless communications,[13] biosensing,[14–16] and nondestructive inspections.[17,18] Metalens can manipulate THz waves and mm-waves with a high degree of freedom, and thus show superiority in broadband focusing,[19] full-space multichannel operation,[20] and aberration-free imaging.[18] Among them, achromatic THz metalenses have attracted intensive attention in the THz band for advanced imaging and biomedical diagnostics.

In addition, metalenses with dynamic functionalities are especially desirable to meet the compact and intelligent needs of THz apparatuses. The functions of metadevices remain static once they are fabricated. To achieve dynamic control, phase-change materials,[21,22] microelectromechanics,[23] 2D materials,[24,25] semiconductors,[26–28] flexible substrates,[29,30] as well as liquid crystals (LCs)[31–36] have been integrated with metasurfaces. Among them, LCs attract special attention due to their broadband birefringence and excellent stimuli responsiveness, and the propagation phase and geometric phase can be manipulated separately via controlling the tilt angle and azimuthal angle of the LCs.

Recently, LC-based tunable THz lenses[37] and self-standing LC polymer lenses[38] have both been presented. LC can also endow metasurfaces with tunability.[34,35] The switchable geometric phase of LC is adopted to dynamically compensate for the linear resonant phase dispersion of a dielectric metalens and thus enable an active manipulation of chromatic dispersion.[39] The switchable geometric phase of LC is also integrated with a metalens to realize the alternation between a spin-selective bifocal state and a polarization-independent single focus state.[40] If the foci of metalens are dynamically tuned or switched, and the achromatic property is maintained, multidepth full-color imaging and multispectral detection can be accomplished within a single snapshot. This approach will significantly enhance the efficiency of THz imaging and inspection and thus fulfills the key requirements for practical utilization in biomedical diagnostics and security screening.

In this work, we propose an LC-enabled varifocal achromatic metalens. The design is based on two key points: first, the dual foci are induced by the basic phase profile combined with a fixed part and a switchable part; second, the group delay of the

Q. Wang, Y. Xu, Z. Guo, W. Hu
National Laboratory of Solid State Microstructures
Key Laboratory of Intelligent Optical Sensing and Manipulation
College of Engineering and Applied Sciences
Nanjing University
Nanjing 210023, China
E-mail: huwei@nju.edu.cn
L. Chen, C. Huang
National Laboratory of Solid State Microstructures
College of Physics
Nanjing University
Nanjing 210093, China
E-mail: huangchunyu@nju.edu.cn
The ORCID identification number(s) for the author(s) of this article can be found under https://doi.org/10.1002/lpor.202501901

DOI: 10.1002/lpor.202501901

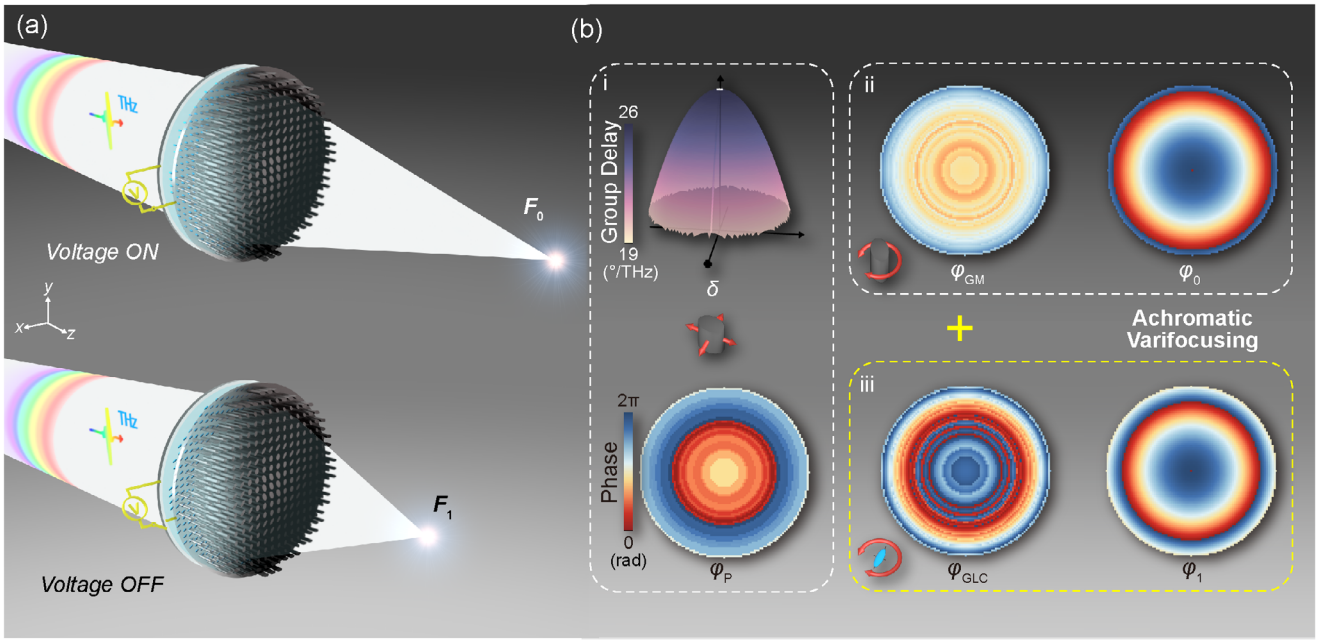

Figure 1. Function and design of the LC-enabled varifocal achromatic metalens. a) Schematic illustration of the LC-enabled varifocal achromatic metalens with focus length of F_0 for voltage ON-state and F_1 for voltage OFF-state; b) Phase decomposition chart of the LC-enabled varifocal achromatic metalens, i. the group delay δ (up) of the metasurface, and the propagation phase φ_P (down) at the central frequency of the metasurface, associated with the shape of the cylindroids; ii. The geometric phase of the metasurface φ_{GM} (left) associated with the rotation of the cylindroids and the target phase compensation diagram φ_0 (right) at the central frequency; iii. The geometric phase of the photopatterned LCs φ_{GLC} (left) and the target phase compensation diagram φ_1 (right) at the central frequency.

propagation phase is properly preset to simultaneously compensate for the diffraction dispersion at the dual foci. The varifocal achromatic metalens is demonstrated in a photopatterned LC-integrated silicon metalens. The metasurface provides both the fixed geometric phase and the propagation phase, whereas the LC supplies the switchable geometric phase. It exhibits excellent achromatic performance at both foci over a broad THz band. Dual-depth multispectral imaging is further verified to present the potential of this varifocal achromatic metalens.

2. Principle and Design

As illustrated in **Figure** 1a, the varifocal achromatic metalens consists of a silicon cylindroid metasurface and a photopatterned LC layer. The former supplies a frequency-dependent propagation phase (φ_P), which results in a positive dispersion caused by the material dispersion of the silicon cylindroid. The metasurface also provides a fixed geometric phase (φ_{GM}), whereas the LC supplies a switchable geometric phase (φ_{GLC}). Both of them are frequency independent and result in a negative diffractive dispersion. If these two opposite dispersions are properly compensated for at both voltage ON (V_{ON}) and voltage OFF (V_{OFF}) states, achromatic focusing could be achieved at the dual foci (Figure 1a).

The phase decomposition process is clearly shown in Figure 1b. The phase profile φ_σ of the varifocal achromatic metalens is depicted as[39]

$$\varphi_\sigma(r,\nu) = \Delta\varphi(r,\nu) + \varphi_{b\sigma}(r) = \delta(r)(\nu-\nu_c) - \frac{2\pi\nu_c}{c}\left(\sqrt{F_\sigma^2+r^2}-F_\sigma\right) \quad (1)$$

where σ is a symbol of bias state ($\sigma = 0$ for V_{ON} and $\sigma = 1$ for V_{OFF}), r represents the radius of an arbitrary point on the lens, ν represents the frequency, $\Delta\varphi$ is the positive dispersion introduced by φ_P, $\varphi_{b\sigma}$ represents the basic phase profile, $\delta(r) = \partial\varphi_\sigma(r)/\partial\nu$ denotes the first-order Taylor item of the phase profile, which is known as the group delay,[41] ν_c denotes the central frequency of the achromatic band, c represents the light velocity in vacuum, and F_σ denotes the focal length. As shown in Figure 1b-i, to offer simultaneous compensation for dual foci, $\Delta\varphi(r)$ should be properly designed by tailoring $\delta(r)$ according to

$$\delta(r) = k - \frac{\pi}{c}\left[\left(\sqrt{F_0^2+r^2}-F_0\right)+\left(\sqrt{F_1^2+r^2}-F_1\right)\right] \quad (2)$$

where k is a constant with no impact on focusing. $\varphi_P(r, \nu_c)$ is settled correspondingly. $\varphi_{b\sigma}$ is composed of three different components:

$$\varphi_{b\sigma}(r) = \varphi_P(r,\nu_c) + \left[\varphi_{GM}(r) - \sigma\varphi_{GLC}(r)\right](-1)^\sigma \quad (3)$$

$\varphi_P(r, \nu_c)$ is a term accompanied by a given δ, which makes a constant contribution to $\varphi_{b\sigma}$. Via properly designing $\Delta\varphi$ to match the diffractive dispersion of $\varphi_{b\sigma}$ ($\sigma = 0, 1$) simultaneously, the LC-integrated metalens can be electrically switched between two foci and exhibit achromatic focusing at both V_{ON} (Figure 1b-ii, $\sigma\varphi_{GLC} = 0$) and V_{OFF} states (Figure 1b-iii). The minus before $\varphi_{GM}(r)$ for $\sigma = 1$ is due to the spin reversion after the beam passes through the LC layer, which works as a half-wave plate (details shown in the Supporting Information).[40]

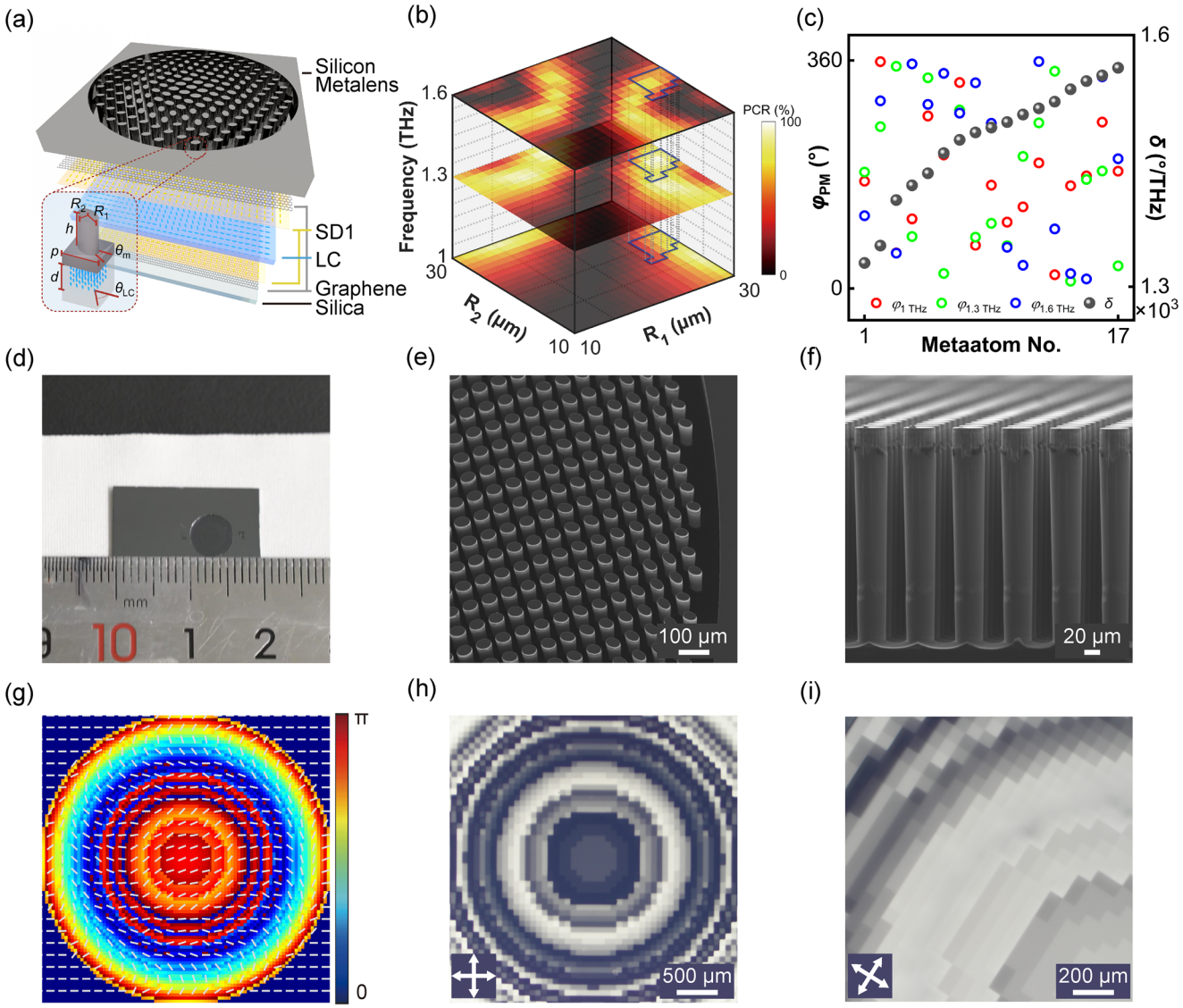

Figure 2. Design and fabrication of the LC-enabled varifocal achromatic metalens. a) Configuration and geometric parameters of the LC-enabled varifocal achromatic metalens. The cylindroid metaatom has a fixed height of h = 300 μm and a lattice period of p = 65 μm with various dimensions of R_1, R_2, and θ_M. b) PCR database of meta-atoms at ν_{min} = 1.0 THz, ν_c = 1.3 THz and ν_{max} = 1.6 THz; c) Group delay and phases of selected meta-atoms; d) Photograph of the fabricated metalens; SEM e) top image and f) cross-sectional image of the silicon metasurface; g) Director distribution of the photopatterned LC; h, i) POM photographs of the photopatterned LC.

To validate the above design, we fabricate an LC-integrated metalens, as illustrated in **Figure** 2a. It features a sandwiched configuration, and the LC is filled in the cell formed by a silicon cylindroid metasurface and a fused silica. Two graphene layers are coated inside the cell to work as transparent electrodes. A set of cylindroid meta-atoms with different major and minor radii R_1 and R_2 are selected and spatially aligned to obtain φ_p, which is linearly related to frequency (Figure S1, Supporting Information). φ_{GM} and φ_{GLC} are twice the azimuth angle of the cylindroid meta-atoms θ_M and LCs θ_{LC}, respectively. According to the polarization conversion efficiency (PCR) database constructed via ANSYS Lumerical FDTD (Figure 2b), meta-atoms with PCR(ν) > 40% are selected (PCR(ν_c) > 70%). The group delay and phases of selected meta-atoms at ν_{min}, ν_c, and ν_{max} are shown in Figure 2c, and their details are shown in Table S1 (Supporting Information). The fabricated metasurface is shown in Figure 2d–f, which exhibits excellent fidelity with the design. The maximum aspect ratio of the fabricated metalens is 8.3. The LC photopatterning is carried out with a digital mask polarization lithography system and the photoalignment agent SD1.[42] Figure 2g shows the designed director distribution of the photopatterned LC. The LC orientations are consistent with the brightness variance under a polarization optical microscope (POM) (Figure 2h,i). Herein, the cell gap d = 350 μm is optimized to reach the highest PCR across the achromatic band. More detailed designs are presented in Figure S2 (Supporting Information).

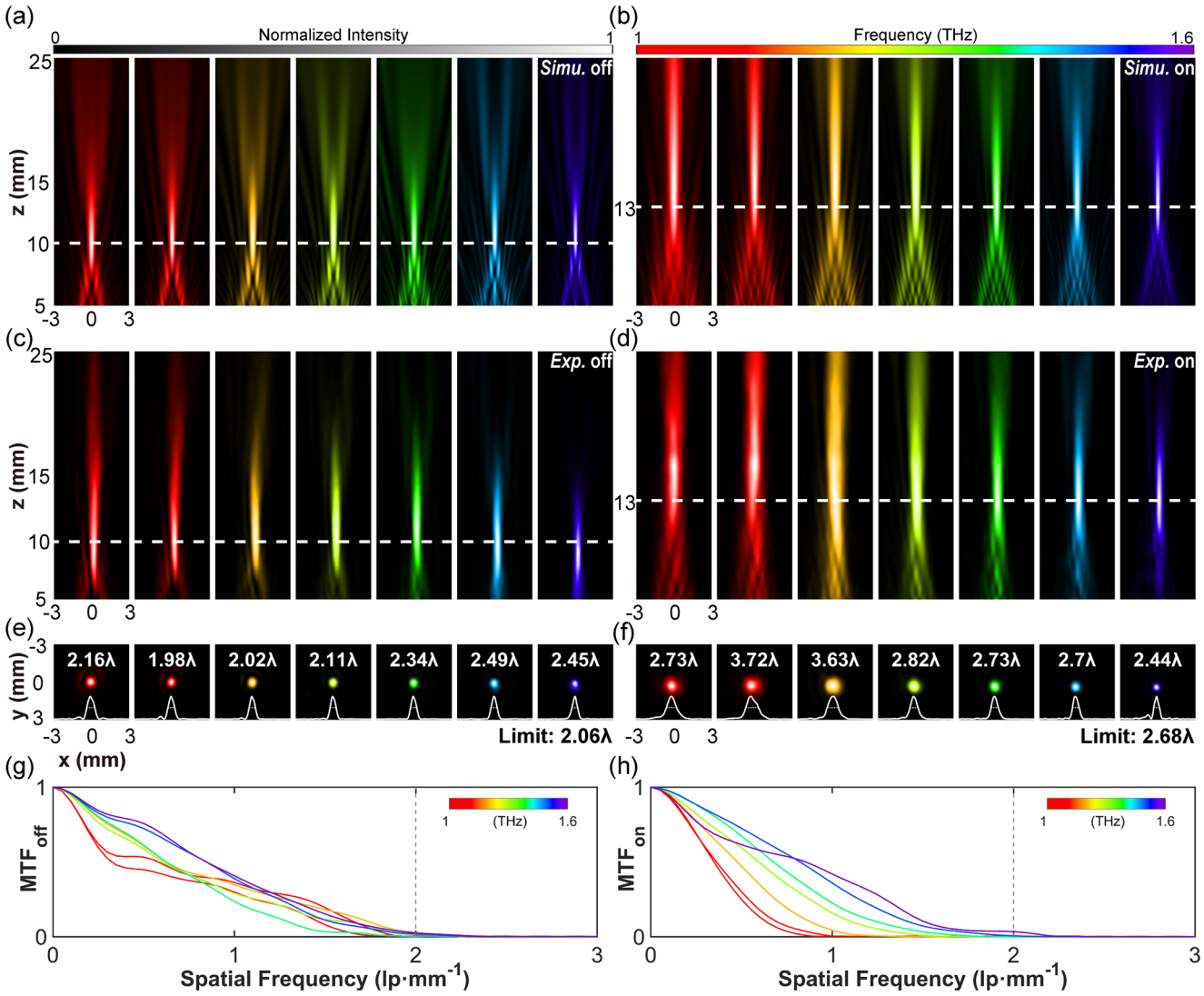

Figure 3. Simulation and characterization of the LC-enabled varifocal achromatic metalens across 1.0–1.6 THz. Simulated focusing properties of the metalens in *z* direction for LCP incidence at a) V_{OFF} and b) V_{ON} states, respectively; Experimental focusing properties of the metalens in *z* direction for LCP incidence at (c) V_{OFF} and d) V_{ON} states, respectively; Foci in *xy* planes and corresponding intensity profiles with FMHW labeled on the top of each image at e) V_{OFF} and f) V_{ON} states, respectively; Modulation transfer function (MTF) of the metalens at g) V_{OFF} and h) V_{ON} states, respectively.

3. Varifocal Achromatic Focusing

We use FDTD to numerically simulate the focusing properties of the LC-integrated metalens. **Figure** 3a,b displays the simulated intensity distribution in *z* direction at V_{OFF} and V_{ON} states for 1.0–1.6 THz LCP incidence. The simulations reveal excellent varifocal achromatic properties over a broad band of 1.0–1.6 THz. To vividly exhibit the different frequencies, they are marked in different colors. A relative working bandwidth of 46.2% with respect to the central frequency is achieved. In the V_{OFF} state, the metalens converges all transmissive THz waves to $F_1 = 10$ mm. In the V_{ON} state, the focus is switched to $F_0 = 13$ mm. The switching time for V_{ON} and V_{OFF} of the LC integrated metalens is 24 and 125 s, respectively. The numerical apertures of the metalens are 0.29 for V_{OFF} and 0.23 for V_{ON}. A scanning near-field THz microscope (SNTM, Figure S3, Supporting Information) is used to examine the dual achromatic foci of the metalens. The measured results along *z* direction at the V_{OFF} and V_{ON} states are presented in Figure 3c,d. Excellent varifocal achromatic properties are verified, and the obtained average focal lengths are $F_1 = 10.20$ mm and $F_0 = 13.76$ mm, respectively, which are consistent with the simulations. The extracted intensity profiles in *xy* planes and the corresponding full width at half maximum (FWHM, represented in the incident wavelength $\lambda = c/\nu$) are shown in Figure 3e,f. The diffractive limitation of the FMHW is calculated as $1.22\lambda F_\sigma / D$, here $D = p \times 91 = 5915$ μm is the diameter of the metalens. The limitation is 2.06λ for V_{OFF} states and 2.68λ for V_{ON} states. The metalens shows FMHWs comparable to the diffraction limit. To further investigate the resolution of the metalens, the modulation transfer functions (MTF) of two states are calculated and shown in Figure 3g,h, respectively. It suggests a resolution up to 1.99 lp·mm^{-1}, which decreases significantly for

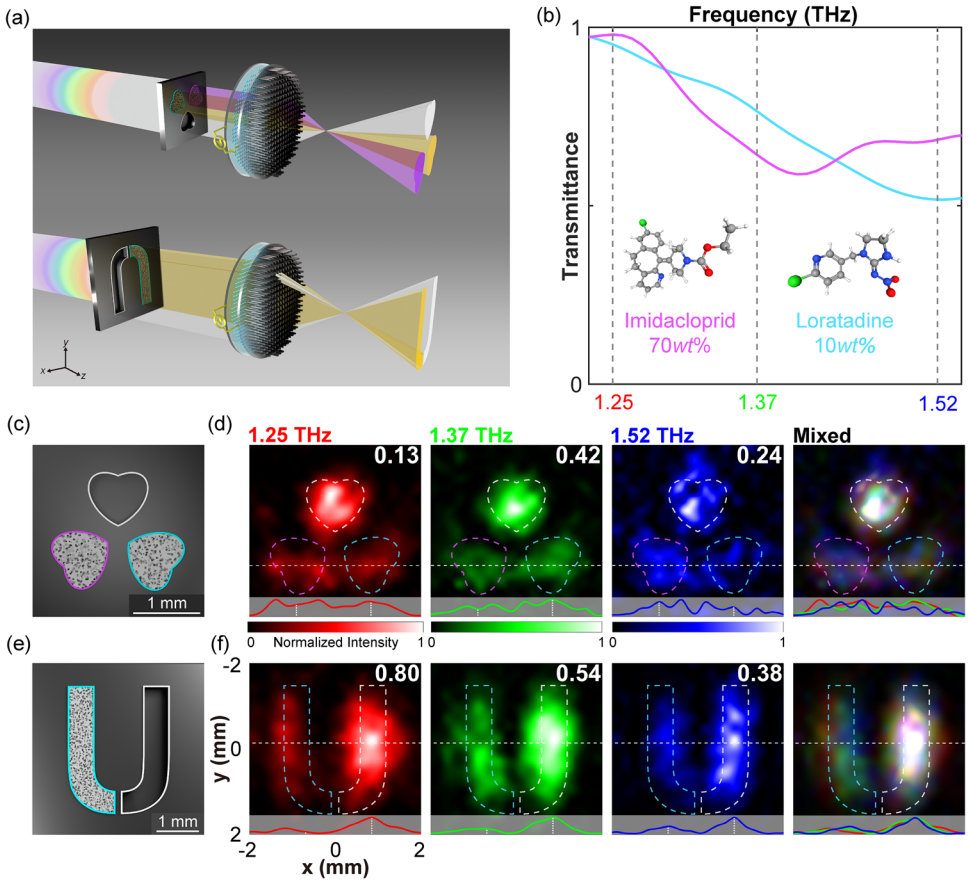

Figure 4. Dual-depth multispectral imaging of the LC-enabled varifocal achromatic metalens. a) Schematic illustration of the dual-depth multispectral imaging of the metalens. The white region is an empty hole, the cray region is a hole with 70 wt.% imidacloprid, and the pink region is a hole with 10 wt.% loratadine; b) Featured transmittances of the two medicaments. Insets show the molecular structures of imidacloprid and loratadine; c) The clover mask for the imaging test; d) Captured images at 1.25, 1.37, and 1.52 THz and a mixed image in the V_{OFF} state, with intensity contrasts between two medicaments labeled on the top-right of monochromic images; e) "U" mask for the imaging test; f) Captured images at 1.25, 1.37, and 1.52 THz and a mixed image in the V_{ON} state, with intensity contrast between the imidacloprid and the empty hole labeled on the top-right of monochromic images. All color bars indicate the normalized intensity.

lower frequencies after bias is applied. The focusing efficiency is defined as the proportion of the concentrated power at the focal plane within a 2×FWHM diameter compared with the incident intensity. Average efficiencies of 23.9% and 26.1% are obtained for the V_{OFF} and V_{ON} states, separately. The proposed varifocal achromatic exhibits comparable performance compared to recently reported THz achromatic metalens (Table S2, Supporting Information)[18,43–45] but has a dynamic switching ability. Further focus performances, such as the modulation transfer functions, focus length variation among different frequencies, NA, and efficiency of the metalens, are presented in Figure S4 (Supporting Information). In summary, the LC-integrated metalens exhibits excellent achromatic focusing properties at dual foci in a range of 1.0–1.6 THz, successfully confirming the feasibility of the proposed design.

4. Dual-Depth Multispectral Imaging for Medicament Identification

To demonstrate the practicality of the LC-enabled varifocal achromatic metalens, dual-depth multispectral imaging for medicament identification is carried out. This experiment aimed to validate a varifocal, achromatic metalens for dual-depth pharmaceutical imaging. The lens successfully distinguished between drugs of similar visible color by analyzing transmittance contrasts, demonstrating its potential for dynamic, non-destructive screening. The experimental setup is shown in **Figure** 4a. Two white medicaments with similar appearances (mass fractions of 70 wt.% imidacloprid and 10 wt.% loratadine) are selected as analytes. They exhibit distinct transmittances in the working band of the LC-integrated metalens (Figure 4b). Notably, 70 wt.% imidacloprid exhibits lower transmittance at 1.37 THz due to the featured absorption, while the minimum transmittance of 10 wt.% loratadine is at 1.52 THz. Hollow "clover" and "U" shaped metal masks fabricated on silicon are adopted as both the medicament holder and the imaging object. The measurements are carried out according to the Gaussian imaging equation $1/F_\sigma = 1/u_\sigma + 1/v$, where u_σ is the object distance and v is the image distance. We fix v to achieve switchable dual-depth imaging. The three frequencies of 1.25, 1.37, and 1.52 THz are marked in red, green, and blue, respectively, to provide a more vivid presentation.

For the measurement in the V_{OFF} state, the "clover" mask is set at u_1 = 16.25 mm, and two leaves are filled with the two medicaments separately (Figure 4c). We use the SNTM to capture images at three characteristic frequencies and v = 26 mm. Figure 4d reveals that three "clover" leaves exhibit different intensity distributions as a result of the different transmittances of the filled analytes. The intensity distributions in monochromatic and mixed images are all consistent with the spatial distributions of analytes. Furthermore, we calculate the intensity contrast between two medicaments by $|I_{imidacloprid} - I_{loratadine}| / (I_{imidacloprid} + I_{loratadine})$ at three separate frequencies, and find larger contrasts are recorded at 1.37 and 1.52 THz. For the V_{ON} state, half of the "U" mask is filled with 70 wt.% imidacloprid (Figure 4e), and the image is captured at $u_0 = v$ = 26 mm. Figure 4f shows a strong contrast between the empty region and the region filled with 70 wt.% imidacloprid. The intensity contrast between imidacloprid and the empty region is calculated by $|I_{imidacloprid} - I_{empty}| / (I_{imidacloprid} + I_{empty})$ at three frequencies. This proves that both the shape and composition of analytes can be detected at two different depths with the LC-enabled varifocal achromatic metalens. It provides a new technique for dynamic nondestructive safety screening and pharmaceutical identification.

5. Discussion

The proposed LC-integrated metalens overcomes the fixed focal length restriction of traditional achromatic metalenses and achieves longitudinal switching between dual foci with chromatic aberration compensation over 1.0–1.6 THz. The strategy can be further expanded to lateral dual achromatic foci with on-demand diffraction angles and focus lengths (Figures S2 and S5, Supporting Information). It breaks the critical barrier in dynamic THz meta-optics. To further improve the focusing efficiency, the absorption and reflection loss of metalens, transparent electrodes, and LCs should be reduced via optimizing the materials and structures, as well as introducing anti-reflection layers. Furthermore, introducing inverse design to optimize the group delay, aberration suppression, and switchable multifunctionalities could be achieved in a broader band.[46–48] Larger variation ranges of numerical aperture and focal length can be realized with hierarchical meta-atom libraries with high aspect-ratio geometries. The switchability can be improved by adopting higher birefringence or faster response LCs. Notably, the techniques used for the proof-of-concept demonstration are also available for scalable production, which may revolutionarily improve the existing THz apparatuses.

Achromatic metalenses with dynamic varifocal capabilities are still challenging to realize. Here, we demonstrate a varifocal achromatic metalens that offers switchable focus while preserving broadband achromaticity. Our device compensates for diffractive dispersion with a predefined propagation phase group delay, combining a fixed geometric phase (from cylindroid meta-atoms) and a switchable one (from photopatterned liquid crystals) for dynamic modulation. With a properly designed LC-integrated metalens, dual achromatic foci (10.20 and 13.76 mm) are dynamically altered via bias across 1.0–1.6 THz. Dual-depth multispectral imaging of masks filled with two medicaments is further verified, revealing its potential for pharmaceutical identification and nondestructive inspection. This work provides a framework for the design and scalable fabrication of planar THz optics with dynamic and adaptive functionalities.

6. Experimental Section

LC-Integrated Metalens Fabrication: Figure S6 (Supporting Information) schematically illustrates the fabrication process for the LC-integrated metalens. The silicon metasurface was fabricated via standard UV photolithography and reactive ion etching. The intrinsic silicon substrate, which is 1.5 × 2.0 mm and 1.0 mm thick with a resistance of ≥5000 Ω·cm, was cleaned sequentially with acetone, ethanol, and ultrapure water, followed by O-plasma cleaning. Hexamethyldisilane (HMDS) was coated on the substrate to enhance adhesion to the photoresist. The photoresist (AZ4620, Merck, Germany) was spin-coated at 1000 rpm for 40 s and then photolithographed with a photolithography instrument (MA6BA6, SUSS Micro Tec, Germany) for 20 s. Reactive ion etching (RIE) was carried out using a deep silicon etching machine (HSE200S, NAURA Co. Ltd., China) for 480 cycles. The residual photoresist was lifted off. The metasurface and silica substrate were ultrasonically cleaned and treated with O-plasma for 5 min. The few-layer graphene (Six Carbon Technology, Shenzhen) was transferred to them and then spin-coated at 3000 rpm for 30 s to coat the photoalignment agent (SD1, NCLCP, China). Afterward, they were baked at 100 °C for 10 min to remove the solvent. Finally, the metasurface and silica substrate were separated by 350-µm-thick Mylars and sealed with glue to form the cell. The cell was exposed via a digital mask polarization lithography system to record the desired patterns. A nematic LC (NC-M-LC101-135, NCLCP, China) with a birefringence of 0.3 during 1.0–1.6 THz was infiltrated into the cell at 180 °C. The imaging mask was fabricated using a standard photolithography mask fabrication procedure and RIE.

Simulations: ANSYS Lumerical FDTD Solutions were used to sweep the parameters to obtain the database of silicon cylindroid meta-atoms. For simplification, only one diameter of the metalens was analyzed to check the focusing property due to the infinite rotational symmetry of the lens. The LC layer beneath the silicon metalens was divided into small cuboid domains with 65 × 65 × 350 µm ($x \times y \times z$) in size. The LC was set as a diagonal dielectric material with diagonal elements of xx and yy equal to 1.6 and diagonal elements of zz equal to 1.9. The LC director distribution was set via an LC orientation module. LCP incidence plane waves at 1.0–1.6 THz propagating along the z-axis were utilized as a source.

Characterizations: An SNTM setup (Terahertz Photonics, China) based on photoconductive THz generation and detection was utilized to evaluate the performance of the LC-integrated metalens. A scanning tip fixed on a motorized stage (JCOPTIX, China) was used to record the field in the xy plane with a step size of 0.3 × 0. 3 mm for focus characterization and 0.3 × 0.3 mm for image characterization. In xz plane, the field was captured with a step size of 0.3 × 1.0 mm. An interpolation algorithm was adopted to analyze the data. A square wave signal with a frequency of 1 kHz and V_{rms} = 230 V was applied as bias.

Supporting Information

Supporting Information is available from the Wiley Online Library or from the author.

Acknowledgements

Q.W. and Y.X. contributed equally to this work. This work was supported by the National Key Research and Development Program of China (2022YFA1203700), the National Natural Science Foundation of China (NSFC) (T2488302 and 62035008), and the Fundamental Research Funds for the Central Universities (021314380244).

Conflict of Interest

The authors declare no conflict of interest.

Data Availability Statement

The data that support the findings of this study are available from the corresponding author upon reasonable request.

Keywords

achromatic metalens, liquid crystal, photoalignment, terahertz, tunable metadevice

Received: July 18, 2025
Revised: September 2, 2025
Published online: September 25, 2025

[1] N. Yu, P. Genevet, M. A. Kats, F. Aieta, J. P. Tetienne, F. Capasso, Z. Gaburro, *Science* **2011**, *334*, 333.
[2] S. Sun, Q. He, S. Xiao, Q. Xu, X. Li, L. Zhou, *Nat. Mater.* **2012**, *11*, 426.
[3] W. T. Chen, A. Y. Zhu, V. Sanjeev, M. Khorasaninejad, Z. Shi, E. Lee, F. Capasso, *Nat. Nanotechnol.* **2018**, *13*, 220.
[4] D. W. Zhang, C. T. Xu, Q. M. Chen, H. Cao, H. G. Yu, Q. G. Tan, Y. Q. Lu, W. Hu, *Photonix* **2024**, *5*, 17.
[5] H. Chung, O. D. Miller, *Opt. Express* **2020**, *28*, 6945.
[6] S. Wang, P. C. Wu, V. C. Su, Y. C. Lai, M. K. Chen, H. Y. Kuo, B. H. Chen, Y. H. Chen, T. T. Huang, J. H. Wang, R. M. Lin, C. H. Kuan, T. Li, Z. Wang, S. Zhu, D. P. Tsai, *Nat. Nanotechnol.* **2018**, *13*, 227.
[7] X. Xiao, Y. Zhao, X. Ye, C. Chen, X. Lu, Y. Rong, J. Deng, G. Li, S. Zhu, T. Li, *Light Sci. Appl.* **2022**, *11*, 323.
[8] M. Choi, J. Kim, S. Moon, K. Shin, S. W. Nam, Y. Park, D. Kang, G. Jeon, K. I. Lee, D. H. Yoon, Y. Jeong, C. K. Lee, J. Rho, *Nat. Mater.* **2025**, *24*, 535.
[9] Q. Chen, Y. Gao, S. Pian, Y. Ma, *Phys. Rev. Lett.* **2023**, *131*, 193801.
[10] Y. Wang, Q. Chen, W. Yang, Z. Ji, L. Jin, X. Ma, Q. Song, A. Boltasseva, J. Han, V. M. Shalaev, S. Xiao, *Nat. Commun.* **2021**, *12*, 5560.
[11] Y. L. Wang, Q. B. Fan, T. Xu, *Opto-Electron. Adv.* **2021**, *4*, 200008.
[12] B. Ferguson, X. C. Zhang, *Nat. Mater.* **2002**, *1*, 26.
[13] L. Wang, J. Y. Dai, K. S. Ding, H. X. Zeng, Q. Cheng, Z. Q. Yang, Y. X. Zhang, T. J. Cui, *Sci. Adv.* **2024**, *10*, adq8693.
[14] B. W. Liu, Y. Peng, Z. M. Jin, X. Wu, H. Y. Gu, D. S. Wei, Y. M. Zhu, S. L. Zhuang, *Chem. Eng. J.* **2023**, *462*, 142347.
[15] J. Feng, X. Wang, W. Shi, L. Ma, Y. Ji, F. Fan, S. Chang, *Nanophotonics* **2024**, *13*, 4007.
[16] N. Zhang, F. Gao, R. Wang, Z. Shen, D. Han, Y. Cui, L. Zhang, C. Chang, C. W. Qiu, X. Chen, *Adv. Mater.* **2025**, *37*, 2411490.
[17] X. L. You, R. T. Ako, S. Sriram, W. Withayachumnankul, *Laser Photonics Rev.* **2025**, *19*, 2401011.
[18] J. Chen, S. X. Huang, K. F. Chan, G. B. Wu, C. H. Chan, *Nat. Commun.* **2025**, *16*, 363.
[19] X. L. He, B. W. Ren, K. F. Chan, A. M. H. Wong, *Laser Photonics Rev.* **2025**, *19*, 2401843.
[20] C. Qi, X. L. He, B. W. Ren, A. M. H. Wong, *Adv. Opt. Mater.* **2024**, *12*, 2302459.
[21] B. Chen, S. Yang, J. Chen, J. Wu, K. Chen, W. Li, Y. Tan, Z. Wang, H. Qiu, K. Fan, C. Zhang, H. Wang, Y. Feng, Y. He, B. Jin, X. Wu, J. Chen, P. Wu, *Light Sci. Appl.* **2023**, *12*, 136.
[22] B. Dong, S. Zhu, G. Guo, T. Wu, X. Lu, W. Huang, H. Ma, Q. Xu, J. Han, S. Zhang, Y. Wang, X. Zhang, L. Huang, *Adv. Mater.* **2025**, *37*, 2417183.
[23] M. Manjappa, P. Pitchappa, N. Singh, N. Wang, N. I. Zheludev, C. Lee, R. Singh, *Nat. Commun.* **2018**, *9*, 4056.
[24] A. Di Gaspare, C. Song, C. Schiattarella, L. H. Li, M. Salih, A. Giles Davies, E. H. Linfield, J. Zhang, O. Balci, A. C. Ferrari, S. Dhillon, M. S. Vitiello, *Nat. Commun.* **2024**, *15*, 2312.
[25] Q. Li, X. Cai, T. Liu, M. Jia, Q. Wu, H. Zhou, H. Liu, Q. Wang, X. Ling, C. Chen, F. Ding, Q. He, Y. Zhang, S. Xiao, L. Zhou, *Nanophotonics* **2022**, *11*, 2085.
[26] S. Han, L. Cong, Y. K. Srivastava, B. Qiang, M. V. Rybin, A. Kumar, R. Jain, W. X. Lim, V. G. Achanta, S. S. Prabhu, Q. J. Wang, Y. S. Kivshar, R. Singh, *Adv. Mater.* **2019**, *31*, 1901921.
[27] J. Zhang, J. Lou, Z. Wang, J. Liang, X. Zhao, Y. Huang, C. Chang, G. Hu, *Adv. Mater.* **2025**, *37*, 2410671.
[28] J. X. Fan, Y. Zhou, Z. Q. Xue, G. Z. Xu, J. L. Chen, H. Y. Xing, D. Lu, L. Q. Cong, *Laser Photonics Rev.* **2025**, *19*, 2401869.
[29] X. Lu, F. Zhang, L. Zhu, S. Peng, J. Yan, Q. Shi, K. Chen, X. Chang, H. Zhu, C. Zhang, W. Huang, Q. Cheng, *Nat. Commun.* **2024**, *15*, 3157.
[30] G. Xu, Z. Xue, J. Fan, D. Lu, H. Xing, P. P. Shum, Y. Zhou, L. Cong, *Adv. Mater.* **2024**, *36*, 2406526.
[31] X. H. Jiang, Y. Y. Ji, F. Fan, S. L. Jiang, Z. Y. Tan, H. J. Zhao, J. R. Cheng, S. J. Chang, *Photonics Res.* **2023**, *11*, 1880.
[32] H. J. Zhao, F. Fan, Y. M. Wang, J. Liu, Y. Y. Ji, J. R. Cheng, S. J. Chang, *Laser Photonics Rev.* **2024**, *18*, 2400442.
[33] S. T. Xu, J. X. Fan, Z. Q. Xue, T. Sun, G. M. Li, J. D. Li, D. Lu, L. Q. Cong, *Photonics Res.* **2024**, *12*, 2207.
[34] H. G. Yu, H. C. Wang, Z. X. Shen, S. N. Tao, S. J. Ge, W. Hu, *Chin. Opt. Lett.* **2023**, *21*, 010002.
[35] S. Wang, H. B. Guo, B. W. Chen, X. Y. Hu, W. Zhu, J. B. Wu, C. H. Zhang, K. B. Fan, H. B. Wang, B. B. Jin, J. Chen, P. H. Wu, *Laser Photonics Rev.* **2024**, *18*, 2301301.
[36] Y. Xu, J. Q. Yang, K. Fan, S. Wang, J. Wu, C. Zhang, D. C. Zhan, W. J. Padilla, B. Jin, J. Chen, P. Wu, *Adv. Sci. (Weinh)* **2024**, *11*, 2406878.
[37] Z. Shen, S. Zhou, S. Ge, W. Duan, L. Ma, Y. Lu, W. Hu, *Opt. Express* **2019**, *27*, 8800.
[38] Z. X. Shen, M. J. Tang, P. Chen, S. H. Zhou, S. J. Ge, W. Duan, T. Wei, X. Liang, W. Hu, Y. Q. Lu, *Adv. Opt. Mater.* **2020**, *8*, 1902124.
[39] Z. X. Shen, S. H. Zhou, X. A. Li, S. J. Ge, P. Chen, W. Hu, Y. Q. Lu, *Adv. Photonics* **2020**, *2*, 036002.
[40] Q. G. Wang, S. J. Ge, H. G. Yu, W. Hu, *Laser Photonics Rev. 2024*, *18*, 2400869.
[41] W. T. Chen, A. Y. Zhu, J. Sisler, Z. Bharwani, F. Capasso, *Nat. Commun.* **2019**, *10*, 355.
[42] P. Chen, B. Y. Wei, W. Hu, Y. Q. Lu, *Adv. Mater.* **2020**, *32*, 1903665.
[43] Y. Xu, J. Q. Gu, Y. F. Gao, Q. L. Yang, W. Y. Liu, Z. B. Yao, Q. Xu, J. G. Han, W. L. Zhang, *Adv. Funct. Mater.* **2023**, *33*, 2302821.
[44] F. Zhao, Z. P. Li, X. M. Dai, X. Y. Liao, S. Li, J. C. Cao, Z. G. Shang, Z. H. Zhang, G. F. Liang, G. Chen, H. Li, Z. Q. Wen, *Adv. Opt. Mater.* **2020**, *8*, 2000842.
[45] Q. Cheng, M. Ma, D. Yu, Z. Shen, J. Xie, J. Wang, N. Xu, H. Guo, W. Hu, S. Wang, T. Li, S. Zhuang, *Sci Bull (Beijing)* **2019**, *64*, 1525.
[46] X. Q. Jiang, W. H. Fan, X. Chen, L. R. Zhao, C. Qin, H. Yan, Q. Wu, P. Ju, *Nanophotonics* **2025**, *14*, 921.
[47] Z. Fan, C. Qian, Y. Jia, M. Chen, J. Zhang, X. Cui, E.-P. Li, B. Zheng, T. Cai, H. Chen, *Phys. Rev. Appl.* **2022**, *18*, 024022.
[48] W. Ma, Z. Liu, Z. A. Kudyshev, A. Boltasseva, W. Cai, Y. Liu, *Nat. Photonics* **2020**, *15*, 77.

